Indonesian Journal of Electrical Engineering and Informatics (IJEEI)
Vol. 13, No. 3, September 2025, pp. 585~600
ISSN: 2089-3272, DOI: 10.52549/ijeei.v13i3.5460

Blind Image Quality Metric for Color Images Based on Human Vision System and Deep CNN

Ali Erdem Altınbaş[1], Yıldıray Yalman[2]
[1]Department of Electronics and Communication Engineering, Kocaeli University, Turkey
[2]Department of Information Systems Engineering, Piri Reis University, Turkey

Article Info

Article history:

Received Feb 21, 2024
Revised Aug 10, 2025
Accepted Aug 27, 2025

Keyword:

blind image quality metric
deep CNN
no-reference image quality assessment
human vision system

ABSTRACT

Abstract: This article introduces a novel blind image quality metric (BIQM) for color images which is designed taking into account human visual system characteristics. The BIQM has a four-stage framework: RGB to YUV transformation, denoising with convolutional neural network , quality evaluation, and weighting to make it compatible with the human visual system. Experimental results, including Spearman's rank-order correlation coefficient, confirm BIQM's effectiveness, particularly in scenarios involving white noise and its compatibility with the human visual system. Furthermore, a survey involving 100 participants ranks images based on three distinct qualities, validating the method's alignment with the human visual system. The comparative analysis reveals that the proposed BIQM can compete with commonly used non-referenced quality measures and is more accurate than some of them. The MATLAB codes for the development of the BIQM are made available through the provided link: https://bit.ly/49MrbFX

Copyright © 2025 Institute of Advanced Engineering and Science.
All rights reserved.

Corresponding Author:

Ali Erdem Altınbaş,
Department of Electronics and Communication Engineering,
Kocaeli University,
Kabaoğlu, Baki Komsuoğlu Bulvarı No:515, Umuttepe, 41001 İzmit/Kocaeli
Email: alierdemaltinbas@gmail.com

1. INTRODUCTION

The determination of perceived image quality by the human eye holds significant importance in visual communication and image processing. In communication systems, digital images undergo a series of processes including digitization, compression, and transmission before reaching the end-user [1]. Moreover, image quality plays a crucial role in the concept of object identification within biomedical imaging, which represents one of the most prevalent applications of image processing [2].

Quality metrics for digital images encompass three distinct measurement methodologies: full-reference (FR), no-reference (NR), and reduced-reference (RR) [3]. RR studies employ partial image information or specific features to assess image quality. FR metrics, widely documented in the literature [4], rely on numerical comparisons but face challenges in integration with the human visual system (HVS). Additionally, a significant limitation of FR studies is their dependence on a reference image for comparison. Prominent examples of FR metrics include Peak Signal to Noise Ratio (PSNR), Structural Similarity (SSIM) [5], and Universal Quality Index (UQI) [6].

In the literature, the frequency of proposals for no-reference (NR) metrics is comparatively lower. Mathematical comparison methods are dysfunctional because there is no reference image in the NR metrics. From this point of view, in the field of NR quality metrics, various studies have been carried out with pattern recognition algorithms and feature extraction methods. For example, Blind Image Quality Index (BIQI) [7], Perception based Image Quality Evaluator (PIQUE) [8], and Blind/Referenceless Image Spatial Quality Evaluator (BRISQUE) [9] have been developed in recent years. One approach utilized in IQAs is the

incorporation of features into the assessment architecture [10]. This approach is supported by existing literature highlighting the significant impact of local or structural features on the determination of image quality [11], [12]. For clarity, the working principles and the NR-IQA categories of some methods used in this study are summarized in Table 1.

Table 1. Working Principles of NR-IQA Metrics Included in the Evaluation

Metric	Category	Working Principle
BLIINDS-II	Transform Domain-based	Uses statistical features of DCT coefficients. Distortions alter DCT statistics, and these changes are used to predict quality.
BRISQUE	Traditional ML (NSS-based)	Extracts Natural Scene Statistics (NSS) features in the spatial domain. Quality scores are predicted using Support Vector Regression (SVR).
BIQI	Early NSS-based	Divides the image into sub-bands, extracts NSS features from each band, and maps them to quality scores via regression.
DIIVINE	Traditional ML (NSS-based)	Extracts NSS-based features, classifies the distortion type first, and then predicts quality using a regression model trained for that distortion category.
NIQE	Traditional ML (NSS-based)	A completely opinion-unaware model. Learns a multivariate Gaussian model of NSS features from natural images and predicts quality without training on human opinion scores.
IL-NIQE	Traditional ML (NSS-based)	An improved version of NIQE with an extended set of NSS features and multiple image categories for better generalization.

In the presented study, the deep convolutional neural network is used. By employing the residual learning method, the proposed approach effectively estimates and removes various types of noise in the image, including gaussian, sharpen, salt and pepper, poisson, and JPEG compression [13]. The image obtained as a result of denoising is accepted as a reference image. Thus, the quality of the image can be determined by using the image and its estimated version. In addition, during the comparison of two images for quality determination, YUV color space is used in order to be more compatible with the HVS.

The novelty of the proposed BIQM lies in the integration of a DnCNN-based denoising stage with HVS-driven feature weighting in the YUV domain. Unlike existing NR-IQA metrics that rely solely on NSS-based or handcrafted features, proposed BIQM first reconstructs a pseudo-reference image through residual learning, and then incorporates the biological sensitivity of the human eye in the final quality estimation. This dual design bridges the gap between deep learning-based denoising and perceptual modeling, providing a more reliable no-reference image quality metric.

The second section of the paper outlines the key components of the proposed blind quality metric, including Deep convolutional neural networks (CNN), HVS, and SSIM. The third section provides a detailed examination of how the quality metric operates. In the fourth section, experimental results are presented, along with comparisons to other methods. The paper concludes with the final section, which offers conclusive findings and perspectives.

2. FUNDAMENTAL THEMES

2.1. Human Vision System (HVS)

Due to certain characteristics of the human visual system (HVS), measuring image quality using the RGB color space may hinder the attainment of accurate results. Figure 1 illustrates the two types of photoreceptors in the human eye, known as rods and cones, which are responsible for detecting light and color, respectively.

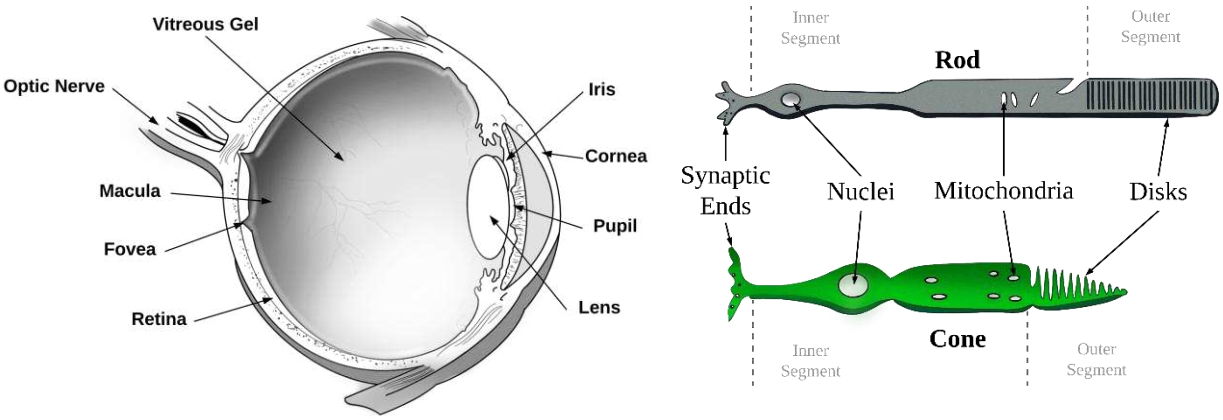

Figure 1. View of the human eye, rod, and cone cells

The retina consists of approximately 120 million rod cells sensitive to luminance, while the number of color-sensitive cone cells is around 7 million. This distribution indicates that approximately 95% of the total cells in the retina are primarily sensitive to luminance, with the remaining 5% dedicated to color perception [14]. Consequently, the impact of luminance on visual perception is more pronounced than that of colors. By conducting quality measurements in the YUV color space, which allows for the separation of light and color information, the measurement results can be aligned with the characteristics of the HVS [15].

2.2. Deep CNN

In the proposed BIQM framework, the denoiser is implemented using the DnCNN (Denoising Convolutional Neural Network) architecture introduced by Zhang et al. [13]. In this model, DnCNN employs a deep convolutional structure with 17–20 layers, which makes it capable of capturing more complex statistical dependencies in image structures (Figure 2). The network design is inspired by the VGG (Visual Geometry Group) architecture and is specifically tailored for image denoising tasks [20].

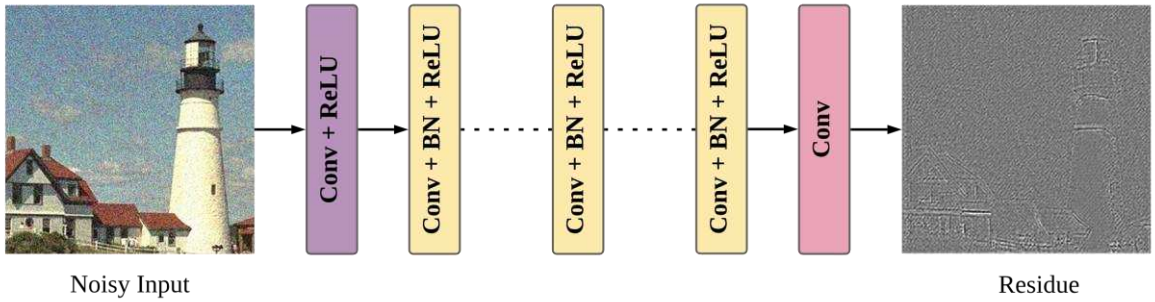

Figure 2. Residue Learning by using DnCNN

The input detoriated image is defined as:

$$y = x + v \tag{1}$$

where y is the distorted image, x is the original clean image, and v denotes the additive noise. Traditional discriminative denoising models aim to learn the mapping function $F(y) = x$, directly predicting the clean image. Instead, DnCNN adopts a residual learning strategy, where the network is trained to approximate the residual mapping (Figure 3):

$$R(y) \approx v \tag{2}$$

$$\overline{v} = y - R(y) \tag{3}$$

Figure 3. Denoising with DnCNN

This formulation simplifies the optimization task, as learning the noise component is generally easier than directly predicting the clean image. To further improve convergence speed and stability, batch normalization (BN) has been integrated into each convolutional block [17]. The combination of residual learning and batch normalization accelerates training and enhances denoising performance.

The objective function is defined as the mean squared error (MSE) between the estimated and the ground-truth residuals:

$$L(\Theta) = \frac{1}{2N}\sum_{i=1}^{N} \| R(y_i;\, \Theta) - (y_i - x_i) \|_F^2 \tag{4}$$

where Θ represents the trainable parameters of the CNN, and N is the number of training samples. This loss guides the network to minimize the discrepancy between the predicted noise and the actual noise, thereby indirectly enhancing the reconstruction quality of the clean image [13].

The success of DnCNN lies in its ability to generalize to various distortion levels, including blind Gaussian denoising, thanks to its deep residual learning design. Although training deep CNNs from scratch can be computationally demanding [16], the use of pre-trained networks significantly reduces the training cost and makes such models practical for real-world applications [18]. Furthermore, utilizing fine-tuning in conjunction with pre-trained networks has been shown in some studies to lead to more favorable outcomes [19].

While DnCNN itself is not the primary contribution of this work, it plays a critical role as a preprocessing stage. By producing denoised images, it ensures that the proposed BIQM can extract human visual system (HVS)-based features more reliably. Consequently, the originality of this study is not in developing a new denoiser, but in integrating the denoised outputs into a novel HVS-driven blind image quality metric.

2.3. Peak Signal to Noise Ratio

PSNR is a ratio obtained by comparing two numerical sequences. During PSNR calculation, the Mean Squared Error (MSE) is first calculated (Eq. (5)). MSE has a long history predating PSNR and has been widely used as a quality metric in signal processing for many years. Originally used for signal fidelity, MSE has also been applied to digital signals with the advent of the computer age [21]. The calculation of MSE involves determining the mean squared differences between two images of size M × N, as defined by:

$$MSE = \frac{1}{MN}\sum_{i=1}^{M}\sum_{j=1}^{N}\left(x_{ij} - y_{ij}\right)^2, \tag{5}$$

x and y can be two different images. The farther these two images are numerically from each other, the MSE will be higher. Based on this, the PSNR can be defined as:

$$PSNR(x,y) = 10log_{10}\left(\frac{255^2}{MSE}\right), \tag{6}$$

The reason 255 is used here is that the bit depth of the image is assumed to be 8, corresponding to 8 bits per pixel. Moreover, it is important to note that higher MSE values result in lower PSNR values [22]. However, PSNR has been subject to scrutiny and ongoing research due to its limited similarity to the human visual system. Consequently, considerable efforts in quality metric research in recent decades have been focused on addressing this limitation [23].

2.4. Structural Similarity

Over the past decades, researchers have explored alternatives to the purely numerical comparison offered by MSE to better align with the characteristics of the human visual system (HVS). In addition to the transmitter, channel, and receiver variables associated with numerical comparison, the HVS, as described in Section 2.2, incorporates visual perception phenomena studied in psychology. Notably, Bovik et al. conducted significant research on this aspect, resulting in the development of SSIM [5]. The SSIM can be expressed in the following formula:

$$SSIM(x,y) = \big(l(x,y)\big)^{\alpha}\big(c(x,y)\big)^{\beta}\big(s(x,y)\big)^{\gamma}, \tag{7}$$

In this expression, *l*, *c*, and *s* correspond to luminance, contrast, and structural components, respectively. When these statements are examined one by one, the luminance is expressed as:

$$l(x,y) = \frac{2\mu_x\mu_y + C_1}{\mu_x^2 + \mu_y^2 + C_1}, \tag{8}$$

μ_x and μ_y are the mean of the image x and y, respectively. The constant C_1 is added to avoid instability when the $2\mu_x\mu_y$ expression is too close to zero. The contrast in the second component of Eq. (7) is expressed as:

$$c(x,y) = \frac{2\sigma_x\sigma_y + C_2}{\sigma_x^2 + \sigma_y^2 + C_2}, \tag{9}$$

Covariances of x and y images are specified as σ_x and σ_y. Finally, the structural component is expressed as:

$$s(x,y) = \frac{\sigma_{xy} + C_3}{\sigma_x\sigma_y + C_3}, \tag{10}$$

As it draws attention, the numerator of the contrast element and the denominator of the structural component are shared by the $\sigma_x\sigma_y$ expression. Therefore, if $\alpha = \beta = \gamma = 1$ and $C_3 = C_2/2$ are considered to simplify Eq. (7), the result is [5]:

$$SSIM(x,y) = \frac{\big(2\mu_x\mu_y + C_1\big)\big(2\sigma_{xy} + C_2\big)}{\big(\mu_x^2 + \mu_y^2 + C_1\big)\big(\sigma_x^2 + \sigma_y^2 + C_2\big)}, \tag{11}$$

SSIM gained prominence upon its initial proposal due to several advantages it offered over PSNR. However, it is important to note that SSIM, as a full-reference image quality metric, requires two images for computation. It assesses the structural similarity between the two images to determine the quality relationship between them.

3. THE PROPOSED METRIC: BIQM

The proposed BIQM comprises four distinct phases, which are outlined below and visualized in Figure 4:

- Phase 1: Image which quality is to be measured is transformed into YUV space,
- Phase 2: CNN is determined according to the file type (.jpeg or .bmp) of the image,
- Phase 3: Denoising is performed by using CNN specified for each color channel. The obtained denoised color channels (Y_d, U_d, V_d) are assumed as reference image color channels,
- Phase 4: Pre-quality results are calculated by comparing the original Y, U, V channels and the Y_d, U_d, V_d channels via the SSIM. Considering the biological properties of the HVS, the pre-quality results are weighted and the final BIQM quality result is obtained.

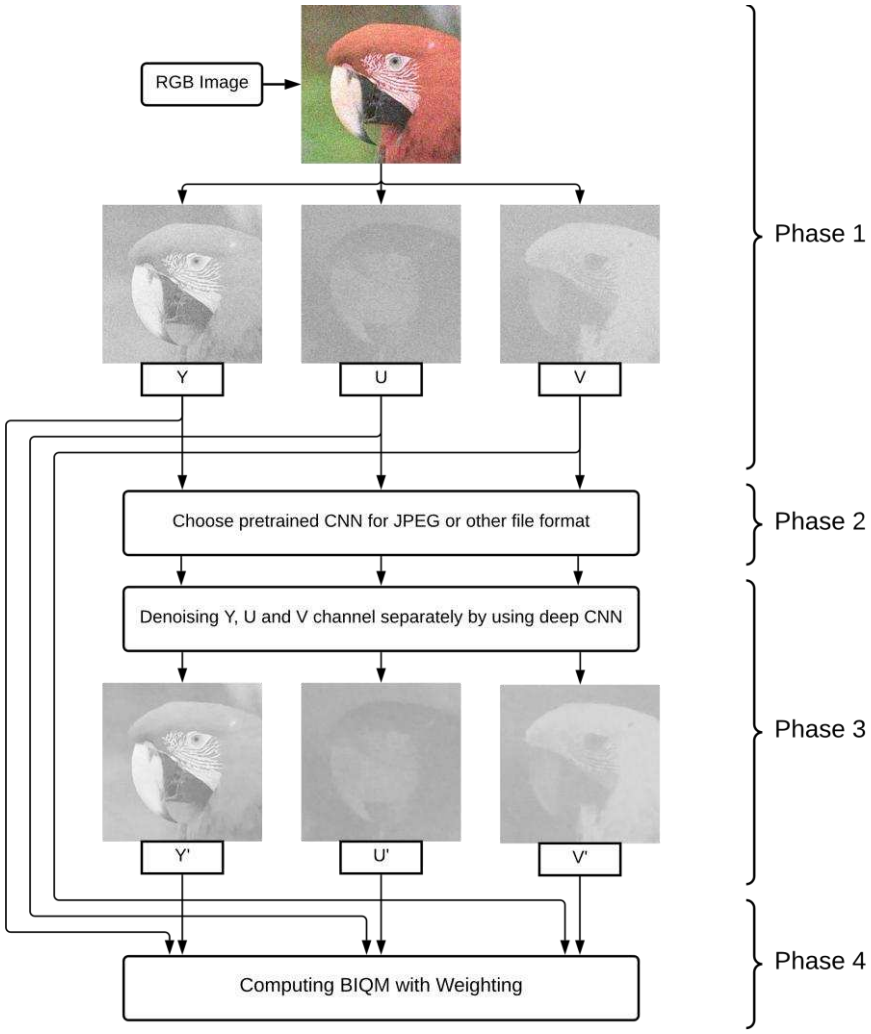

Figure 4. Flowchart of the proposed BIQM

3.1. Phase 1: YUV Transformation Process

In this phase, the image whose quality is to be measured is transformed into YUV space. The decision to transform the image into the YUV color space is based on the understanding that the Y channel, which represents the luminance information, holds greater importance in terms of human visual perception [24]. The equation used to separate (or make independent) luminance information from color information is expressed as:

$$\begin{aligned} Y &= 0.257R + 0.504G + 0.098B + 16 \\ U &= -0.148R - 0.291G + 0.439B + 128 \\ V &= 0.439R - 0.386G - 0.071B + 128 \end{aligned} \quad (12)$$

The process of returning from YUV space to RGB space involves utilizing specific transformation formulas. These formulas, which are given in [25], facilitate the conversion of the YUV representation back to the RGB color space:

$$\begin{aligned} G &= 1.1644(Y - 16) + 1.596(V - 128) \\ R &= 1.164(Y - 16) - 0.813(V - 128) - 0.391(U - 128) \\ B &= 1.164(Y - 16) + 2.018(U - 128) \end{aligned} \quad (13)$$

The constants used in Eq. (9) and Eq. (10) correspond to the standard coefficients of the RGB to YUV color space conversion as defined in widely adopted video and image processing standards ITU-R BT.601 [52]. In this study, the transformation was performed to prioritize the luminance information, as it plays a crucial role in visual perception. The purpose of this conversion was to ensure that the luminance channel

receives appropriate weighting compared to the color channels, taking into account its greater significance in determining image quality.

3.2. Phase 2: Choosing Network

It has been shown in previous studies that the blocking effect caused by JPEG should be examined with a separate concept considering the denoising process [26]. The blocking effect because of compression, especially at low bit rates, is sometimes examined separately [27]. Although most of the commonly used types of generated noise can be classified on a statistical basis, the blocking effect, a kind of compression problem, must be considered from a different perspective [28]. Because it is a noise caused by the quantification of DCT coefficients during compression [29]. From this point of view, two different pre-trained CNNs have been used in this study. Then, separate pre-trained CNNs would be used for JPEG and other noise types.

The use of pre-trained CNN has a direct effect on the result in most cases. The use of a properly trained network is often of great importance in structures that require forecasting. In addition to this, the use of multiple pre-trained CNNs is an issue that has been investigated in recent years [30]. Because training a CNN is a challenging process in terms of time and calculation costs. In order to overcome this problem, the use of the GPU, which is very successful in matrix operations, is being examined with the parallel programming concept, and research on performance analysis continues [16]. The main purpose of using pre-trained CNN in this study is to avoid training cost. The training and test data of the CNN used are described below.

3.2.1. Training and Testing the CNN

The pre-trained network used in the proposed model had been trained using the Berkeley segmentation dataset [31]. For the training, 400 images of 180×180 size were used. It has been noted that using more images for training did not provide a worthwhile improvement to the training cost. In that study, three noise levels had been used to train DnCNN for Gaussian denoising with known noise levels: $\sigma = 15$, 25 and 50. The patch size as 40 × 40, and crop 128 × 1,600 patches were set to train the model. In addition, to train a single DnCNN model for blind Gaussian denoising, Zhang et al. set the range of the noise levels as $\sigma \in [0, 55]$. The patch size as 50×50 and the crop 128×3,000 patches were set to train the model [13].

Two different datasets were used for test images in the BIQM. The first is the Berkeley segmentation dataset (BSD68) which is depicted above, the second is the 12 images which are detailed in the study of Zhang et al. [13]. In addition, test images are not included in the training dataset.

As mentioned above, a separate model is trained for JPEG. To generate the JPEG deblocking input, the image is compressed with a quality factor ranging from 5 to 99 using the MATLAB JPEG encoder. 128×8000 image patch (size 50×50) pairs are generated for training. Operations on the patch pairs based on rotation/flip are used during mini-batch learning.

3.3. Phase 3: Denoising with Deep CNN

The more successful this denoising process, which is used to develop the intended quality metric, the more successful it will be to predict the quality. For this reason, the denoising method used is extremely important. The method proposed by Zhang et al. (2015) has proven to be more successful than previous studies [13][10]. In addition, the feedforward denoising CNN developed by them gives a fast result if it is operated with a pre-trained network. Even if it is not pre-trained, the developed network is fully compatible with GPU parallel programming.

The utilization of pre-trained sets in MATLAB enables efficient and effective denoising processes. The selection of the denoising level is predefined and not customizable by the user. These functions are relatively new and do not offer input parameters for fine-tuning denoising applications according to desired rates. To enhance the quality prediction performance, one can consider increasing the number of denoising iterations or retraining the model using transfer learning techniques. While there are multiple methods to enhance denoising performance, it is important to note that the primary objective of this study is to propose an image quality metric rather than focusing on denoising techniques.

3.4. Phase 4: Weightening by the HVS

In the fourth phase, an FR quality metric SSIM is used for quality calculation. However, when using the SSIM, the denoised image is assumed as a reference image in the BIQM. This measurement is made in the YUV color space to suit the HVS. In addition, as mentioned in Section 2.2, the ratio between light and color-sensitive cells in the human eye should also be reflected in the Y and UV channels [52]. For this reason, the quality of the Y channel in the measurement result is 95% effective compared to the human eye, while only 5% of the average of the U and V channels are effective [14].

As a result, the image quality to be determined using the presented method expressed as:

$$BIQM = SSIM(Y,Y') \times 0.95 + [(SSIM(U,U') + SSIM(V,V'))/2] \times 0.05 \quad (14)$$

With this calculation, a color image, it is possible to determine the quality without a reference image.

4. EXPERIMENTAL RESULTS

During the evaluation of the experimental outcomes, it was observed that the proposed method achieved notable efficacy specifically in handling white noise. To further validate the performance of the method, correlation calculations were conducted not only on the widely utilized LIVE [32], CSIQ [33], and TID2013 [34] databases but also on additional databases TID2008 [35] and VCL@FER [36]. This broader selection of databases allowed for a more comprehensive assessment of the method's effectiveness across different noise levels.

These databases encompass a range of characteristics such as varying numbers of observers contributing to the determination of mean opinion scores (MOS), different quantities of reference and noisy images, diverse image sizes, and distinct levels of distortion given in Table 2. These variations in the databases contribute to the diversity and richness of the data available for evaluation and enable a comprehensive analysis of the proposed method's performance across a wide range of conditions.

Table 2. Characteristics of databases used in the study

Database	Reference Image	Distorted Image	Image Size	Distortion Level	Observers
LIVE	20	779	866×591	9	161
CSIQ	30	866	512×384	4-5	25
TID2013	25	3000	512×384	4	985-971
TID2008	25	1700	512×384	7-8	838
VCL@FER	30	866	512×512	4-5	25

To assess the degree of compatibility of the proposed study with the human visual system, the Spearman rank-ordered correlation coefficient (SROCC) and Pearson linear correlation coefficient (PLCC) coefficients were computed. These coefficients measure the degree of correlation between the proposed method's output and human perceptual judgments. A value closer to 1 for these coefficients indicates a stronger correlation between the proposed method and the human visual system. Table 3 provides the ground truth values for the study at hand on the LIVE database [32]. The numeric suffixes "1" and "3" represent the number of times the algorithm was executed on the Y channel. Additionally, the columns labeled as "JPEG" denote the usage of alternative pre-trained convolutional neural networks for JPEG compression.

Table 3. Spearman rank-ordered correlation coefficient (SROCC) and Pearson linear correlation coefficient (PLCC) comparison of proposed BIQM on individual distortions types on the LIVE database.

	SROCC-1	SROCC-3	SROCC-1 JPEG	SROCC-3 JPEG	PLCC-1	PLCC-3	PLCC-1 JPEG	PLCC-3 JPEG
JP2K	0.87237	0.86775	0.90121	0.85892	0.68843	0.74361	0.85593	0.82028
JPEG	0.87759	0.83079	0.82710	0.71597	0.64191	0.67912	0.81639	0.71417
White Noise	0.98198	0.98239	-	-	0.95907	0.96331	-	-
Gaussian Blur	0.73353	0.63188	-	-	0.63065	0.65520	-	-
Fast Fading	0.51002	0.55511	-	-	0.02816	-0.05217	-	-
Average	0.79510	0.77358			0.58964	0.59781		

Upon initial examination, the table illustrates the efficacy of the denoising method for both white noise and compression noise. However, the observed correlation for Gaussian blur and fast fading is comparatively lower due to the inherent blurring effect of the denoising process, particularly in repetitive scenarios. However, it is evident that using a CNN specifically trained for JPEG compression yields improved results for images that have undergone compression, such as those in the JP2k and JPEG formats.

The experimental studies have demonstrated the notable success of the proposed method, particularly in white noise. To thoroughly investigate this aspect, an in-depth analysis was conducted on the state-of-the-art LIVE, CSIQ, and TID2013 databases, focusing specifically on white noise. In order to ensure a fair evaluation, fifteen different IQAs were assessed, and the SROCC results are given in Table 4. It is noted that the proposed BIQM produces scores ranging from 0 to 1, where higher values indicate superior perceived quality and lower values correspond to more significant distortions.

Table 4. Comparative Analysis of SROCC Values for IQAs Across Different Databases

IQA METHODS	LIVE	CSIQ	TID2013
DIIVINE [37]	0.979	0.940	0.906
BLIINDS-II [38]	0.941	0.922	0.741
NIQE [39]	0.961	0.835	0.852
IL-NIQE [40]	0.977	0.866	0.904
CORNIA [41]	0.979	0.941	0.935
BRISQUE [9]	0.978	0.957	0.900
GMLOG [42]	0.97S	0.943	0.946
NFERM [43]	0.980	0.938	0.931
FRIQUEE [44]	0.975	0.941	0.950
BJLC [45]	0.986	0.962	0.959
HOSA [46]	0.975	0.604	0.853
BIECON [47]	0.980	0.902	0.717
WaDIQAm [1]	0.982	0.974	0.843
DB-CNN [48]	0.980	0.948	0.790
Proposed BIQM	**0.981**	**0.951**	**0.919**

Table 5 presents the SROCC results obtained from various IQAs for white noise in the TID2008 and VCL@FER databases. These databases, although less commonly used nowadays, contain a variety of image characteristics and noise types that can provide valuable insights into the performance of IQAs.

The performance of the proposed BIQM was compared against 14 cutting-edge NR-IQA methods across a range of benchmark datasets. As demonstrated in Table 4, BIQM exhibits robust performance on the LIVE, CSIQ, and TID2013 databases, achieving SROCC values of 0.981, 0.951, and 0.919, respectively. The values obtained are consistently competitive with, or in some cases superior to, leading NR metrics such as BRISQUE, BLIINDS-II, NIQE, and CORNIA. It is noteworthy that BIQM demonstrates a high degree of robustness for white noise distortions, aligning closely with the human visual system (HVS) perception.

Furthermore, the results presented in Table 5 offer additional verification of the proposed approach's generalisation ability, utilising the TID2008 and VCL@FER datasets. In this study, the BIQM model demonstrated its capability to achieve correlation values of 0.869 (TID2008) and 0.882 (VCL@FER), which exceed the performance of conventional NR metrics such as BIQI and NIQE. Furthermore, the BIQM model exhibited a comparable or superior performance to BRISQUE in these datasets.

These comparisons demonstrate that the proposed BIQM not only competes with but also surpasses several well-established NR-IQA models across diverse datasets. The consistent results observed across five distinct benchmark databases underscore the robustness, generalisation, and practical applicability of BIQM. This comprehensive evaluation directly addresses the concern regarding performance comparison with other methods and strengthens the claim that BIQM offers a novel and effective solution for blind image quality assessment.

In addition to the ground truth evaluation, peer-based PSNR tests were conducted to compare the image quality. The test set consisted of images with various types of commonly used noise, including Gaussian, Poisson, salt & pepper, sharpen, and JPEG. While the PSNR metric described in Section 2.4 failed to sort the images based on their quality, the presented metric allowed for accurate ranking of the images from the highest to the lowest quality. To enhance the visibility of noise effects, selected parts of the images were enlarged during the comparison.

Table 5. Comparative Analysis of SROCC Values for IQAs on TID2008 and VCL@FER Databases.

	TID2008	VCL@FER
BLIINDS-II [38]	0.779	0.894
DIIVINE [37]	0.812	0.913
BRISQUE [9]	0.853	0.823
NIQE [39]	0.786	0.848
BIQI [7]	0.798	0.703
QAC [49]	0.707	0.882
Proposed BIQM	0.869	0.882206

As stated above, according to the PSNR, which is an FR metric, all images in Fig. 5 have the same PSNR value (28.29 dB). However, this is not a suitable situation for the HVS, and quality difference between images is perceived. In addition, the original image may not be available, so the use of the NR metrics is inevitable. It is also shown in Table 5 that other NR quality metrics mentioned in the introduction section do not give satisfactory results.

According to the BIQI, the PIQUE, and the BRISQUE metrics used in comparisons, when the image quality result approaches 0, it is assumed that the visual quality of the image increases. On the contrary, when the BIQM result approaches 0, the visual quality of the image decreases.

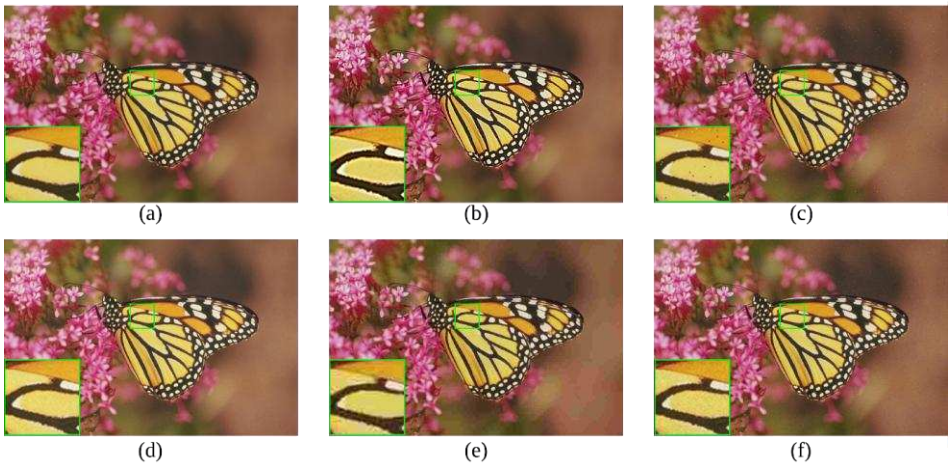

Figure 5. Comparison of "Monarch" images with different types of distortions, all with PSNR = 28.29 dB: (a) Original image. (b) Sharpen image. (c) Salt & Pepper image. (d) Poisson image. (e) JPEG image. (f) Gaussian image.

Figure 5 and Table 6 show that the PIQUE and the BRISQUE metrics exhibit limitations in accurately determining the impact of salt & pepper, JPEG, and gaussian noises, as well as differentiating between salt & pepper and Gaussian noise. Despite the fact that the HVS perceives the Gaussian noisy image as the worst in terms of visual quality, the these metrics suggest that it has the best image quality among the different types of noise.

Table 6. Performance comparisons of NR image quality metrics for Monarch image.

	BIQI	PIQUE	BRISQUE	**Proposed BIQM**
Sharpen	5.937	14.891	10.777	0.9863
S&P	13.774	**37.777**	**32.144**	**0.9554**
Poisson	21.104	23.784	25.751	0.9531
JPEG	31.810	**58.476**	**53.689**	**0.9229**
Gaussian	32.220	**34.930**	**30.017**	**0.8587**

Another example is presented in Figure 6 with images prepared in the same PSNR value (29.30 dB). Comparison results are given in Table 7.

Table 7. Performance comparisons of NR image quality metrics for Parrot image.

	BIQI	PIQUE	BRISQUE	**Proposed BIQM**
Sharpen	**13.622**	17.869	12.998	**0.9725**
Poisson	21.710	23.369	**21.684**	**0.9549**
S&P	**13.179**	34.132	**16.137**	**0.9528**
JPEG	58.217	**78.061**	48.961	0.9225
Gaussian	30.622	**43.677**	31.687	0.8600

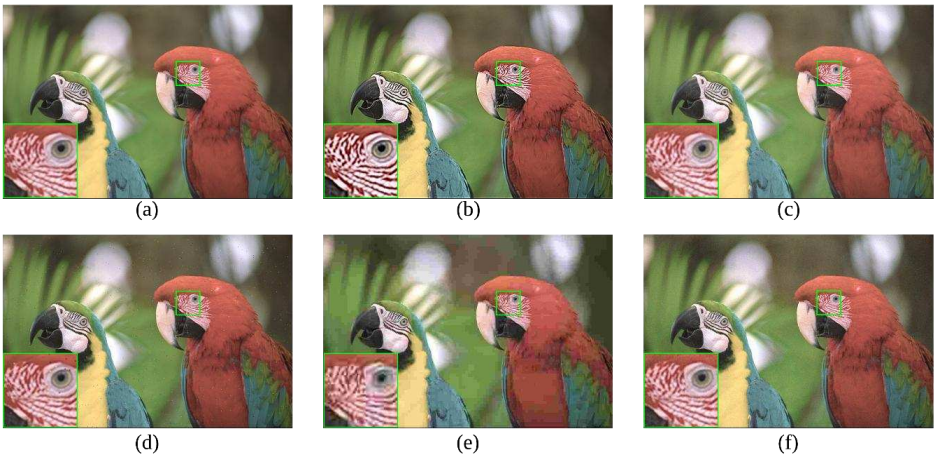

Figure 6. Comparison of "Parrot" images with different types of distortions, all with PSNR = 29.30 dB: (a) Original image. (b) Sharpen image. (c) Poisson image. (d) Salt & Pepper image. (e) JPEG image. (f) Gaussian image.

As shown in Table 7, while the BIQI struggled to distinguish between sharpen and salt & pepper noise, the BIQM yielded a successful result under HVS in this regard. Similarly, the PIQUE failed to separate JPEG and Gaussian noises, and the BRISQUE failed to separate Poisson and salt & pepper noises.

Even if the quality measurement scenario is FR, the PSNR values are equal (i.e., 24.15 dB), on the contrary, the BIQM can distinguish digital images by considering the HVS as seen in Figure 7. Table 8 gives performance comparisons of NR methods and the BIQM method (all noisy images have the same PSNR (24.15 dB) values).

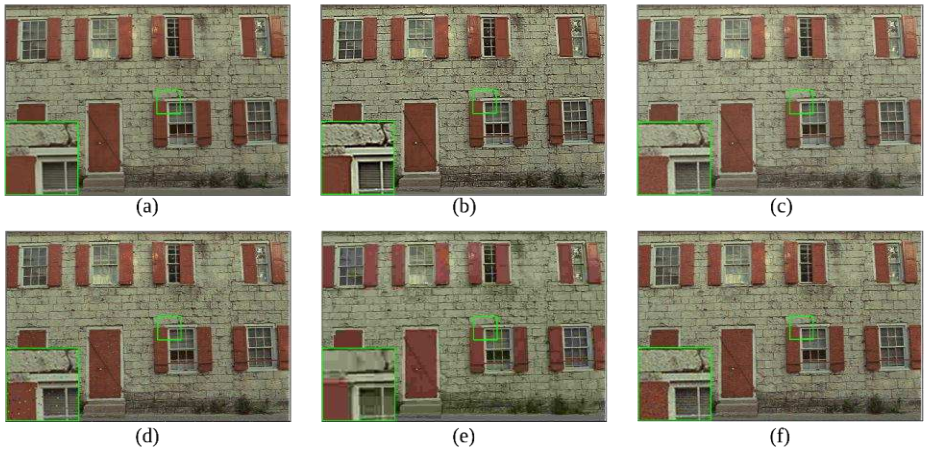

Figure 7. Comparison of "Wall" images with different types of distortions, all with PSNR = 24.15 dB: (a) Original image. (b) Sharpen image. (c) Poisson image. (d) Salt & Pepper image. (e) JPEG image. (f) Gaussian image.

Table 8. Performance comparisons of NR image quality metrics for Wall image.

	BIQI	PIQUE	BRISQUE	**Proposed BIQM**
Sharpen	**39.640**	**54.590**	**32.861**	**0.9697**
Poisson	33.094	47.891	**32.245**	**0.9145**
S&P	31.690	51.913	50.338	0.9025
JPEG	62.707	64.784	63.948	0.8198
Gaussian	**41.810**	**56.012**	39.287	**0.8113**

The results obtained from the BIQI and PIQUE methods indicate that the quality values of sharpened and Gaussian images are similar, while the quality values of sharpened and Poisson images are close according to the BRISQUE method. However, these results do not align with the HVS. In contrast, visual examination reveals that the Gaussian and sharpened images exhibit significant differences. The BIQM metric supports this perceptually noticeable result with its measurement outcomes.

Table 9 presents the comparative performance of various NR image quality metrics, including the BIQM, BIQI, PIQUE, and BRISQUE, on different noisy images. The noisy variations within each image have the same PSNR values, namely Flowers (30.87 dB), House (26.22 dB), and Whitewater (25.73 dB). While sharpened noise produces less quality deterioration at the same PSNR than other types of noise, some NR image quality metrics fail to accurately distinguish between them.

Similarly, other NR image quality metrics exhibit instability in differentiating salt & pepper and gaussian noise. However, visual examination of the noisy images in Fig. 5, Fig. 6, and Fig. 7, in the context of the HVS, shows that salt & pepper and gaussian images differ significantly in quality at the same PSNR value, and the BIQM confirms these results. The corresponding images used in the assessments of Table 9 are shown in Figure 8.

Table 9. Performance comparison of NR image quality metrics for different noisy images. I1, I2, and I3 as Flowers, House, and Whitewater respectively.

		Sharpen	Poisson	S&P	Gaussian	JPEG
I1	BIQI	26.268	17.228	21.912	23.962	43.799
	PIQUE	27.477	18.369	43.507	25.775	65.467
	BRISQUE	20.051	22.893	32.576	24.981	56.814
	Proposed BIQM	**0.9906**	**0.9727**	**0.9696**	**0.9320**	**0.9084**
I2	BIQI	14.935	28.202	26.055	38.721	55.287
	PIQUE	37.516	38.985	32.567	54.400	74.276
	BRISQUE	31.585	29.097	41.455	36.245	61.439
	Proposed BIQM	**0.9695**	**0.9136**	**0.9108**	**0.7855**	**0.8531**
I3	BIQI	38.096	27.753	26.742	39.313	51.228
	PIQUE	32.644	31.164	31.683	44.590	61.161
	BRISQUE	19.378	14.874	53.989	25.267	58.942
	Proposed BIQM	**0.9801**	**0.9437**	**0.9456**	**0.8348**	**0.8266**

I_1 I_2 I_3

Figure 8. Images compared in Table 8. I_1, I_2, and I_3 are Flowers, House, and Whitewater, respectively.

A survey was conducted to understand the effect of the presented method and measure its compatibility with the HVS. In this survey conducted with 100 participants, random participants were asked to rank 3 different images given in Figure 9 according to their quality.

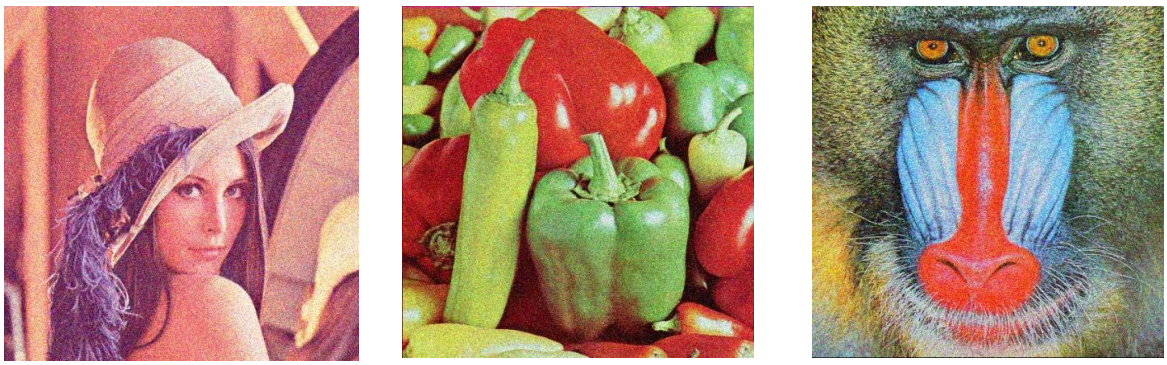

(a) (b) (c)

Figure 9. Images on which the survey was conducted. (a) Lena. (b) Peppers. (c) Baboon.

The sorting of these three images, each of which added a different amount of noise, was made with a strict distinction among the participants. Based on the survey results presented in Figure 10, a clear majority of the participants ranked the image in Figure 9; (a) as the worst quality, followed by (b) and then (c) as the best quality.

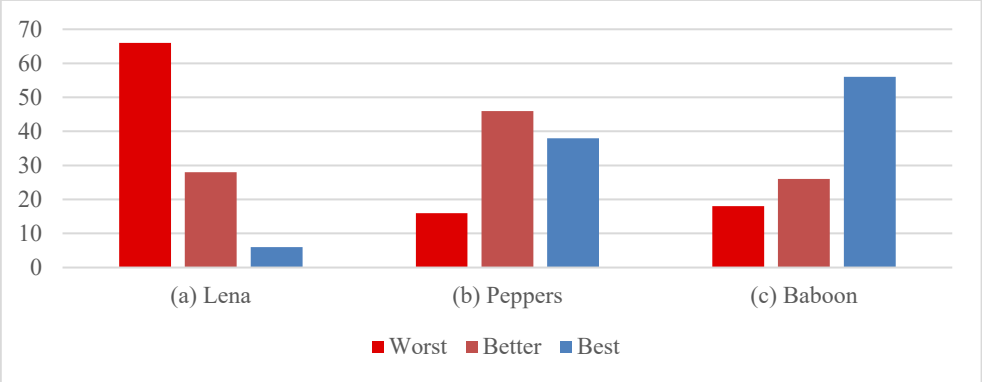

Figure 10. Result of the survey.

According to the evaluations of the participants, a majority of respondents (66 out of 100) rated Lena as the image with the lowest perceived quality. Similarly, 46 participants considered Peppers to be the median-quality image, while 56 participants ranked Baboon as the image with the highest perceived quality. These findings provide insights into the subjective assessment of the images in Figure 9. Additionally, the quality measurements of these images using NR-IQAs are presented in Table 10.

Table 10. NR-IQA results of survey images.

Images / IQA	BIQI	PIQUE	BRISQUE	**Proposed BIQM**
Lena	59.7726	68.4288	44.5229	**0.4031**
Peppers	58.4485	66.1915	42.0760	**0.4453**
Baboon	59.3933	67.4209	46.3070	**0.5576**

When considering the collective findings from Table 9 and Figure 10 it can be observed that the BIQM demonstrates strong compatibility with the human visual system (HVS). Conversely, the results obtained from the application of the BIQI, PIQUE, and BRISQUE metrics to the Peppers image do not align well with the HVS. Furthermore, the survey conducted indicates that utilizing the proposed BIQM as a no-reference quality metric is more preferable in terms of user satisfaction and its alignment with visual perception.

5. CONCLUSION

This study proposes a new deep CNN-based NR image quality metric (BIQM) consisting of four phases, including RGB to YUV transform, CNN determination considering the file type, denoising with deep-CNN, and quality value calculation. The experimental results demonstrate the effectiveness of the presented method, particularly for white noise. The SROCC values indicate that BIQM provides more consistent results in terms of HVS compared to its counterparts, particularly for images corrupted with white noise. Moreover, the survey results suggest that BIQM could potentially enhance user satisfaction when used for image quality measurement.

Another important finding of this survey, consistent with the results of some studies in recent years, is the challenge of distinguishing between low-level and high-level noise images [50, 51]. For future research, investigating the relationship between the amount of noise and the human visual system presents an area of growing interest. Furthermore, with the advancements in CNN models, developing new high-accuracy metrics that do not require human scoring is becoming an increasingly important research area.

On the other hand, when performance evaluation is made, using pre-trained CNN ensures that it operates in a reasonable time even for low-medium level hardware. Performance improvement is possible with the use of advanced GPUs and CPUs. In this way, a fit-for-purpose deep CNN can be trained using a larger and more suitable data set. Finally, the method of working in YUV space and weighting these channels will go further with the development of the concepts of vision and visual perception for future works.

In brief, the main contribution of this work is the integration of DnCNN residual learning with HVS-based channel weighting. This combination improves the robustness of BIQM against various distortions. Unlike existing NR-IQA models, which usually rely only on handcrafted features or lack perceptual weighting, our BIQM bridges deep denoising and perceptual modeling. As a result, it provides a more perceptually consistent and generalizable solution for blind image quality assessment.

The computational complexity of the presented algorithm has been tested only when MATLAB R2022b is running. Technicial Specifications; Intel® Alder Lake Core™ i5-12500H 12C/16T; 18MB L3; E-CORE Max 3.30GHZ E-CORE Max 4.5GHZ;45W;10nm, nVIDIA® GeForce® RTX3050 TI Max-Performance 4GB GDDR6 128-Bit DX12, 32GB (1x32GB) DDR4 1.2V 3200MHz SODIMM, 500GB PCIe M.2 2280 3.0 x4 (R: 2050 MB/s - W: 940 MB/s). Under these conditions, the presented work is completed in an average of 1.252 seconds. With the parallel pool, this time is reduced to 1.103 seconds.

REFERENCES

[1] S. Bosse, D. Maniry, K. R. Müller, T. Wiegand, and W. Samek, "Deep Neural Networks for No-Reference and Full-Reference Image Quality Assessment," IEEE Transactions on Image Processing, vol. 27, no. 1, pp. 206–219, 2018, doi: 10.1109/TIP.2017.2760518.

[2] N. Tajbakhsh et al., "Convolutional Neural Networks for Medical Image Analysis: Full Training or Fine Tuning?," IEEE Trans Med Imaging, vol. 35, no. 5, pp. 1299–1312, May 2016, doi: 10.1109/TMI.2016.2535302.

[3] L. Ma, S. Li, F. Zhang, and K. N. Ngan, "Reduced-reference image quality assessment using reorganized DCT-based image representation," IEEE Trans Multimedia, vol. 13, no. 4, pp. 824–829, 2011, doi: 10.1109/TMM.2011.2109701.

[4] M. Khosravy, N. Patel, N. Gupta, and I. K. Sethi, "Image Quality Assessment: A Review to Full Reference Indexes," in Recent Trends in Communication, Computing, and Electronics, A. Khare, U. S. Tiwary, I. K. Sethi, and N. Singh, Eds., Singapore: Springer Singapore, 2019, pp. 279–288.

[5] Z. Wang, A. C. Bovik, H. R. Sheikh, and E. P. Simoncelli, "Image Quality Assessment: From Error Visibility to Structural Similarity," IEEE Transactions on Image Processing, vol. 13, no. 4, pp. 600–612, 2004, doi: 10.1109/TIP.2003.819861.

[6] Z. Wang and A. C. Bovik, "A Universal Image Quality Index," IEEE Signal Process Lett, vol. 9, no. 3, pp. 81–84, Mar. 2002, doi: 10.1109/97.995823.

[7] A. K. Moorthy and A. C. Bovik, "A two-stage framework for blind image quality assessment," Proceedings - International Conference on Image Processing, ICIP, vol. 17, no. 5, pp. 2481–2484, 2010, doi: 10.1109/ICIP.2010.5651745.

[8] N. Venkatanath, D. Praneeth, B. H. Maruthi Chandrasekhar, S. S. Channappayya, and S. S. Medasani, "Blind image quality evaluation using perception based features," 2015 21st National Conference on Communications, NCC 2015, pp. 1–6, 2015, doi: 10.1109/NCC.2015.7084843.

[9] T. Sun, X. Zhu, J. S. Pan, J. Wen, and F. Meng, "No-reference image quality assessment in spatial domain," Advances in Intelligent Systems and Computing, vol. 329, no. 12, pp. 381–388, 2015, doi: 10.1007/978-3-319-12286-1_39.

[10] X. Jiang, L. Shen, L. Yu, M. Jiang, and G. Feng, "No-reference screen content image quality assessment based on multi-region features," Neurocomputing, vol. 386, pp. 30–41, Apr. 2020, doi: 10.1016/j.neucom.2019.12.027.

[11] X. Jiang, L. Shen, Q. Ding, L. Zheng, and P. An, "Screen content image quality assessment based on convolutional neural networks," J Vis Commun Image Represent, vol. 67, Feb. 2020, doi: 10.1016/j.jvcir.2019.102745.

[12] Z. Wang, L. Shen, Z. Wang, Y. Lin, and Y. Jin, "Generation-based Joint Luminance-Chrominance Learning for Underwater Image Quality Assessment," IEEE Transactions on Circuits and Systems for Video Technology, Mar. 2022, doi: 10.1109/TCSVT.2022.3212788.

[13] K. Zhang, W. Zuo, Y. Chen, D. Meng, and L. Zhang, "Beyond a Gaussian denoiser: Residual learning of deep CNN for image denoising," IEEE Transactions on Image Processing, vol. 26, no. 7, pp. 3142–3155, 2017, doi: 10.1109/TIP.2017.2662206.

[14] S. Toprak and Y. Yalman, "A new full-reference image quality metric based on just noticeable difference," Comput Stand Interfaces, vol. 50, no. June 2016, pp. 18–25, 2017, doi: 10.1016/j.csi.2016.08.003.

[15] Y. Yalman and I. Ertürk, "A new color image quality measure based on YUV transformation and PSNR for human vision system," Turkish Journal of Electrical Engineering and Computer Sciences, vol. 21, no. 2, pp. 603–612, 2013, doi: 10.3906/elk-1111-11.

[16] X. Li, G. Zhang, K. Li, and W. Zheng, "Chapter 4 - Deep Learning and Its Parallelization," in Big Data, R. Buyya, R. N. Calheiros, and A. V. Dastjerdi, Eds., Morgan Kaufmann, 2016, pp. 95–118. doi: https://doi.org/10.1016/B978-0-12-805394-2.00004-0.

[17] B. Moons, D. Bankman, and M. Verhelst, Embedded Deep Learning. 2019. doi: 10.1007/978-3-319-99223-5.

[18] S. N. Narayanan, K. Khanna, B. K. Panigrahi, and A. Joshi, "Chapter 11 - Security in Smart Cyber-Physical Systems: A Case Study on Smart Grids and Smart Cars," in Smart Cities Cybersecurity and Privacy, D. B. Rawat and K. Z. Ghafoor, Eds., Elsevier, 2019, pp. 147–163. doi: https://doi.org/10.1016/B978-0-12-815032-0.00011-1.

[19] X. Jiang, L. Shen, G. Feng, L. Yu, and P. An, "An optimized CNN-based quality assessment model for screen content image," Signal Process Image Commun, vol. 94, May 2021, doi: 10.1016/j.image.2021.116181.

[20] K. Simonyan and A. Zisserman, "Very deep convolutional networks for large-scale image recognition," 3rd International Conference on Learning Representations, ICLR 2015 - Conference Track Proceedings, pp. 1–14, 2015.
[21] Z. Wang and A. C. Bovik, "Error : Love It or Leave It ?," no. January, pp. 98–117, 2009.
[22] D. R. I. M. Setiadi, "PSNR vs SSIM: imperceptibility quality assessment for image steganography," Multimed Tools Appl, vol. 80, no. 6, pp. 8423–8444, 2021, doi: 10.1007/s11042-020-10035-z.
[23] H. R. Sheikh and A. C. Bovik, "Image information and visual quality," IEEE Transactions on Image Processing, vol. 15, no. 2, pp. 430–444, 2006, doi: 10.1109/TIP.2005.859378.
[24] M. Tkalcic and J. F. Tasic, "Colour spaces: perceptual, historical and applicational background," in The IEEE Region 8 EUROCON 2003. Computer as a Tool., 2003, pp. 304–308 vol.1. doi: 10.1109/EURCON.2003.1248032.
[25] Y. Yalman, "Histogram based perceptual quality assessment method for color images," Comput Stand Interfaces, vol. 36, no. 6, pp. 899–908, 2014, doi: 10.1016/j.csi.2014.04.002.
[26] S. Naveen and V. A. Aiswarya, "Image Denoising by Fourier Block Processing and Wiener Filtering," Procedia Comput Sci, vol. 58, pp. 683–690, 2015, doi: 10.1016/j.procs.2015.08.088.
[27] Z. Xiong, M. T. Orchard, and Y. Q. Zhang, "A deblocking algorithm for JPEG compressed images using overcomplete wavelet representations," IEEE Transactions on Circuits and Systems for Video Technology, vol. 7, no. 2, pp. 433–437, 1997, doi: 10.1109/76.564123.
[28] H. C. Burger, C. J. Schuler, and S. Harmeling, "Image denoising: Can plain neural networks compete with BM3D?," Proceedings of the IEEE Computer Society Conference on Computer Vision and Pattern Recognition, pp. 2392–2399, 2012, doi: 10.1109/CVPR.2012.6247952.
[29] C. Chen, Z. Xiong, X. Tian, Z. J. Zha, and F. Wu, "Real-World Image Denoising with Deep Boosting," IEEE Trans Pattern Anal Mach Intell, vol. 42, no. 12, pp. 3071–3087, 2020, doi: 10.1109/TPAMI.2019.2921548.
[30] J. Guérin, S. Thiery, E. Nyiri, O. Gibaru, and B. Boots, "Combining pretrained CNN feature extractors to enhance clustering of complex natural images," Neurocomputing, vol. 423, pp. 551–571, 2021, doi: https://doi.org/10.1016/j.neucom.2020.10.068.
[31] D. Martin, C. Fowlkes, D. Tal, and J. Malik, "A database of human segmented natural images and its application to evaluating segmentation algorithms and measuring ecological statistics," in Proceedings Eighth IEEE International Conference on Computer Vision. ICCV 2001, 2001, pp. 416–423 vol.2. doi: 10.1109/ICCV.2001.937655.
[32] H. R. Sheikh, A. C. Bovik, L. Cormack, and Z. Wang, "Laboratory for Image and Video Engineering - The University of Texas at Austin." https://live.ece.utexas.edu/research/quality/ (accessed May 24, 2021).
[33] D. M. Chandler, "Most apparent distortion: full-reference image quality assessment and the role of strategy," J Electron Imaging, vol. 19, no. 1, p. 011006, Jan. 2010, doi: 10.1117/1.3267105.
[34] N. Ponomarenko et al., "Image database TID2013: Peculiarities, results and perspectives," Signal Process Image Commun, vol. 30, pp. 57–77, Jan. 2015, doi: 10.1016/j.image.2014.10.009.
[35] N. Ponomarenko et al., "TID2008-A Database for Evaluation of Full-Reference Visual Quality Assessment Metrics."
[36] A. Zaric et al., "VCL@FER Image Quality Assessment Database," 2011.
[37] A. K. Moorthy and A. C. Bovik, "Blind image quality assessment: From natural scene statistics to perceptual quality," IEEE Transactions on Image Processing, vol. 20, no. 12, pp. 3350–3364, Dec. 2011, doi: 10.1109/TIP.2011.2147325.
[38] M. A. Saad, A. C. Bovik, and C. Charrier, "Blind image quality assessment: A natural scene statistics approach in the DCT domain," IEEE Transactions on Image Processing, vol. 21, no. 8, pp. 3339–3352, 2012, doi: 10.1109/TIP.2012.2191563.
[39] A. Mittal, R. Soundararajan, and A. C. Bovik, "Making a 'completely blind' image quality analyzer," IEEE Signal Process Lett, vol. 20, no. 3, pp. 209–212, 2013, doi: 10.1109/LSP.2012.2227726.
[40] L. Zhang, L. Zhang, and A. C. Bovik, "A Feature-Enriched Completely Blind Image Quality Evaluator," 2015. [Online]. Available: www.comp.polyu.edu.hk/
[41] P. Ye, J. Kumar, L. Kang, and D. Doermann, "Unsupervised feature learning framework for no-reference image quality assessment," in Proceedings of the IEEE Computer Society Conference on Computer Vision and Pattern Recognition, 2012, pp. 1098–1105. doi: 10.1109/CVPR.2012.6247789.
[42] W. Xue, X. Mou, L. Zhang, A. C. Bovik, and X. Feng, "Blind image quality assessment using joint statistics of gradient magnitude and laplacian features," IEEE Transactions on Image Processing, vol. 23, no. 11, pp. 4850–4862, Nov. 2014, doi: 10.1109/TIP.2014.2355716.
[43] K. Gu, G. Zhai, X. Yang, and W. Zhang, "Using Free Energy Principle for Blind Image Quality Assessment," IEEE Trans Multimedia, vol. 17, no. 1, pp. 50–63, Jan. 2015, doi: 10.1109/TMM.2014.2373812.
[44] D. Ghadiyaram and A. C. Bovik, "Perceptual quality prediction on authentically distorted images using a bag of features approach," J Vis, vol. 17, no. 1, 2017, doi: 10.1167/17.1.32.
[45] Q. Li, W. Lin, K. Gu, Y. Zhang, and Y. Fang, "Blind image quality assessment based on joint log-contrast statistics," Neurocomputing, vol. 331, pp. 189–198, Feb. 2019, doi: 10.1016/j.neucom.2018.11.015.
[46] J. Xu, P. Ye, Q. Li, H. Du, Y. Liu, and D. Doermann, "Blind image quality assessment based on high order statistics aggregation," IEEE Transactions on Image Processing, vol. 25, no. 9, pp. 4444–4457, Sep. 2016, doi: 10.1109/TIP.2016.2585880.
[47] J. Kim and S. Lee, "Fully Deep Blind Image Quality Predictor," IEEE Journal on Selected Topics in Signal Processing, vol. 11, no. 1, pp. 206–220, Feb. 2017, doi: 10.1109/JSTSP.2016.2639328.
[48] W. Zhang, K. Ma, J. Yan, D. Deng, and Z. Wang, "Blind Image Quality Assessment Using A Deep Bilinear Convolutional Neural Network," Jul. 2019, doi: 10.1109/TCSVT.2018.2886771.

[49] W. Xue, L. Zhang, and X. Mou, "Learning without human scores for blind image quality assessment," in Proceedings of the IEEE Computer Society Conference on Computer Vision and Pattern Recognition, 2013, pp. 995–1002. doi: 10.1109/CVPR.2013.133.
[50] W. Zhang, K. Ma, G. Zhai, and X. Yang, "Uncertainty-Aware Blind Image Quality Assessment in the Laboratory and Wild," May 2020, doi: 10.1109/TIP.2021.3061932.
[51] K. Ma, X. Liu, Y. Fang, and E. P. Simoncelli, "Blind Image Quality Assessment by Learning from Multiple Annotators," in 2019 IEEE International Conference on Image Processing (ICIP), 2019, pp. 2344–2348. doi: 10.1109/ICIP.2019.8803390.
[52] ITU-R BT.601-7, *Studio encoding parameters of digital television for standard 4:3 and wide-screen 16:9 aspect ratios*, International Telecommunication Union, Geneva, Switzerland, Mar. 2011.

BIOGRAPHIES OF AUTHORS

Ali Erdem Altinbas, He received the B.Sc. and M.Sc. degree from Piri Reis University, Turkey, in 2020 and 2022, respectively He will get his Ph.D. degree from Kocaeli University in 2026.He is currently working as a system engineer in telecommunication field. His active research interests are steganography, image processing, audio processing, virtual studio technology (VST), and artificial intelligence.

Yildiray Yalman, He received the M.Sc. and Ph.D. degree from Kocaeli University, Turkey, in 2007 and 2010, respectively. He is currently working as a full-time Professor at Piri Reis University in Turkey. His active research interests are data hiding, steganography, image processing, and real-time multimedia communications.